Available online at www.sciencedirect.com
ScienceDirect
Polymer 49 (2008) 1066–1075
polymer
www.elsevier.com/locate/polymer

Cross-linking in polypyrrole and poly(*N*-methylpyrrole): Comparative experimental and theoretical studies

Carlos Alemán [a,*], Jordi Casanovas [b], Joan Torras [c], Oscar Bertrán [c], Elaine Armelin [a], Ramón Oliver [d], Francesc Estrany [d,*]

[a] *Departament d'Enginyeria Química, E.T.S. d'Enginyers Industrials, Universitat Politècnica de Catalunya, Diagonal 647, 08028 Barcelona, Spain*
[b] *Departament de Química, Escola Politècnica Superior, Universitat de Lleida, c/Jaume II no 69, 25001 Lleida, Spain*
[c] *Departament d'Enginyeria Química, EUETII, Universitat Politècnica de Catalunya, Pça. Rei 15, 08700-Igualada, Spain*
[d] *Unitat de Química Industrial, Escola Universitària d'Enginyeria Tècnica Industrial de Barcelona, Universitat Politècnica de Catalunya, Comte d'Urgell 187, 08036 Barcelona, Spain*

Received 22 November 2007; received in revised form 20 December 2007; accepted 21 December 2007
Available online 8 January 2008

Abstract

A comparative study about cross-linking in electrogenerated polypyrrole and poly(*N*-methylpyrrole) is presented. Experimental studies on polymer films prepared under a constant potential of 1.4 V but considering different polymerization times as well as quantum mechanical calculations on model oligomers indicated that cross-linking is very low in polypyrrole, while cross-links are frequently formed by poly(*N*-methylpyrrole) chains. These behaviors have been attributed to the architecture of the molecular chains, which is completely different for the two systems under study. Thus, polypyrrole forms linear chains with some irregularities in the inter-ring linkages, while branched molecules with many irregularities are the most stable for poly(*N*-methylpyrrole). These remarkable differences are fundamentally due to the steric repulsions induced by the methyl groups of poly(*N*-methylpyrrole).

Keywords: Conducting polymer; Cross-linking; Polypyrrole

1. Introduction

Conducting polymers can be prepared electrochemically, by applying a potential across a solution containing the monomer to be polymerized and an electrolyte, or chemically, using oxidants or cross-coupling catalysts. One of the advantages of electrochemical polymerization is that the yielded polymer, which is electrodeposited as a film on the anode, does not need to be isolated and purified. However, anodic electropolymerization has a serious disadvantage: the electrogenerated polymers present structural irregularities, especially cross-linking.

The nucleation and growth mechanism leading to electrodeposition of the polymer on the anode were elucidated using a number of experimental techniques [1–7]. Deposition of long, well-ordered chains onto the electrode surface is followed by growth of either long, flexible chains, or shorter, more cross-linked chains, depending upon both the polymerization conditions and the chemical nature of the monomer.

The degree of cross-linking is typically determined by the number of electrons consumed to incorporate a monomer into the polymer and to oxidize the resulting chain (n_{ox}); this information being determined through the electropolymerization kinetics, *i.e.* by considering different polymerization times for the generation of polymer films under a constant potential [8]. After discounting the oxidation charge used to compensate the charge of the dopant ion of n_{ox}, the average number of electrons per monomer (n_{av}) incorporated into a linear polymer chain obtained from a typical condensation

* Corresponding authors.
E-mail addresses: carlos.aleman@upc.edu (C. Alemán), francesc.estrany@upc.edu (F. Estrany).

0032-3861/$ - see front matter © 2008 Elsevier Ltd. All rights reserved.
doi:10.1016/j.polymer.2007.12.039

mechanism should be $n_{av} = 2.00$, *i.e.* two protons and two electrons are involved in the formation of the α–α bond between the terminal monomeric unit of the chain and the incorporated monomer [7,9]. Thus, cross-links are probed when $n_{av} > 2.00$. Furthermore, the presence of cross-linking is typically accompanied by a reduction of the electrochemical stability, *i.e.* the electroactivity decreases with the number of oxidation–reduction cycles.

In recent studies we used this procedure to detect the presence of cross-linking in two poly(thiophene) derivatives: poly(3,4-ethylenedioxythiophene) [8] and poly(α-tetrathiophene) [10]. As expected, long linear and regular chains were found for poly(3,4-ethylenedioxythiophene) since the dioxane moiety is fused to the β and β′ positions of the thiophene ring [8]. Consistently, the electrochemical stability determined for this material was very high. In contrast, a monomeric unit of poly(α-tetrathiophene) consumes $n_{av} = 3.17$ electrons during its incorporation into the polymer [10]. This means that each monomeric unit forms ca. three linkages to the polymer chain, involving its α- and β-carbon, since it requires one electron to yield a new carbon–carbon bond. Under these conditions, polymer chains are expected to be cross-linked, containing α–α linkages produced during the electrochemical incorporation of new monomeric units as well as α–β and/or β–β linkages giving rise to cross-linking.

In the present study we examine and compare the formation of cross-links in poly(*N*-methylpyrrole) and polypyrrole, hereafter denoted PNMPy and PPy (Scheme 1). In spite of these materials only differ in the methyl substituent at the N-position, their electrochemical properties are significantly different [11–13]. In order to investigate this relevant aspect of PNMPy and PPy, we combine both experimental and theoretical methods. More specifically, the electropolymerization kinetics and electrochemical stability of PNMPy and PPy were studied under identical experimental conditions, while the tendency of *N*-methylpyrrole (NMPy) and pyrrole (Py) containing oligomers to form linkages different from the α–α ones was investigated using quantum chemical methods.

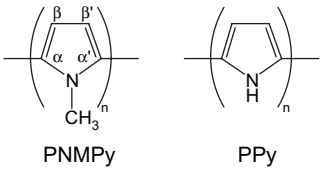

PNMPy PPy

Scheme 1.

2. Methods

2.1. Experimental procedures

Py, NMPy and acetonitrile of analytical reagent grade were purchased from Aldrich and used as-received. Anhydrous lithium perchlorate, analytical reagent grade, from Aldrich was stored in an oven at 80 °C before its use in the electrochemical trials.

PPy and PNMPy films were prepared by chronoamperometry (CA) using a VersaStat II potenciostat–galvanostat connected to a PC computer controlled through a Power Suite Princeton Applied Research Program. All electrochemical experiments were conducted in a three-electrode two-compartment cell under nitrogen atmosphere (99.995% in purity) at 25 °C. The working compartment was filled with 40 mL of a 10 mM monomer solution in acetonitrile with 0.1 M $LiClO_4$. The cathodic compartment was filled with 10 mL of the same electrolyte solution. Steel AISI 316 sheets of 4 cm^2 area were employed as working and counter electrodes. Before each trial, electrodes were cleaned with acetone and dried in an air-flow. The reference electrode was a Ag|AgCl electrode containing a KCl saturated aqueous solution ($E_0 = 0.222$ V *vs.* standard hydrogen electrode at 25 °C), which was connected to the working compartment through a salt bridge containing the electrolyte solution. All potentials (E) given in this work are referred to this electrode. Analyses on the electroactivity of PPy and PNMPy were performed using cyclic voltammetry (CV).

The thickness of the films (l) was estimated from the mass of polymer deposited in the electrode, m_{pol}, which was obtained using the following relation:

$$m_{pol} = Q_{pol}\left(\frac{m}{Q}\right) \tag{1}$$

where Q_{pol} is the polymerization charge (in millicoulombs per centimeter square) consumed in the generation of each layer and (m/Q) the current productivity. The volume of polymer deposited in the electrode (V_{pol}) was obtained using the values of m_{pol} and the densities of PNMPy and PPy. Accordingly, the thickness of each layer was calculated considering the surface of polymerization (S_{pol}), which is the surface of the electrode (4 cm^2), and V_{pol}.

The density of the oxidized polymers was determined by the flotation method from CCl_4/C_2H_5I mixtures, in which they are insoluble.

The values of n_{ox} have been determined using the procedure described in our previous works [8,11,14]. For this purpose the following equation has been used:

$$n_{ox} = \frac{MQ_{pol}}{FW_{ox}\left(1 - W_{dop}\right)} \tag{2}$$

where M is the molar mass of PPy and PNMPy, Q_{pol} is the polymerization charge consumed in each process (in millicoulombs per centimeter square) that was calculated on each chronoamperogram, F is the Faraday constant, W_{ox} is the film weight (in milligram per centimeter square) and W_{dop} is the mass of ClO_4^- per polymer unit of mass. The percentage of ClO_4^- in each collected sample was obtained from reduction of approximately 2 mg of polymer with carbon, followed by determination of the amount of chloride ions released by standard ion chromatography. This analysis was performed with a Kontron 600 HPLC liquid chromatograph fitted with a Waters IC-Pak anion column at 30 °C and equipped with a Wescan conductimetric detector. After discounting the oxidation charge used to compensate the charge of the doping ion, n_{ox} was transformed into n_{av}.

2.2. Theoretical calculations

The most accepted mechanism of pyrrole electropolymerization, which was proposed by Diaz and co-workers [7–9], has been considered for calculations on radical cation species of Py- and NMPy-containing oligomers. The first step of this mechanism, which was confirmed by Waltman and Bargon [15,16] through theoretical calculations based on the correlation between the reactivity and the unpaired electron density of the radical cations, is described in Fig. 1. Quantum mechanical calculations were performed on the radical cation of oligomers containing n heterocyclic rings (nPy$^{\bullet+}$ and nNMPy$^{\bullet+}$) with $n = 2$–4. For each oligomer we consider not only the structures obtained by forming α,α-linkages, which are depicted in Fig. 1, but also the structures derived from couplings in the available β- and β′-position of the Py and NMPy (see next section). Thus, the stability of the nPy$^{\bullet+}$ and nNMPy$^{\bullet+}$ structures with linkages different from the α,α ones will be related with the tendency of PPy and PNMPy to form cross-links.

Full geometry optimizations of all the structures considered for nPy$^{\bullet+}$ and nNMPy$^{\bullet+}$ with $n = 2$–4 were performed at the Unrestricted Hartree–Fock (UHF) level combined with the 6-31 + G(d) [17] basis set, *i.e.* UHF/6-31 + G(d). Previous studies indicated that this simple methodology is able to provide a satisfactory description of the molecular geometry and relative energy for the minimum energy conformations of heterocyclic oligomers like those studied in this work [18–20]. In all cases the inter-ring dihedral angles of the generated structures were initially arranged in *anti* ($\theta = 180.0°$), even although complete geometry optimization was allowed.

The π–π* lowest transition energy (ε_g) was approximated as the difference between the highest occupied molecular orbital (HOMO) and the lowest unoccupied molecular orbital (LUMO) energies, *i.e.* $\varepsilon_g = \varepsilon_{LUMO} - \varepsilon_{HOMO}$. Although UHF calculations provide a satisfactory qualitative description of the electronic properties of polyheterocyclic molecules, we are aware that this method tends to overestimate the ε_g [11,19,21]. Accordingly, the values presented in this work for this electronic property should be considered from a qualitative point of view only. On the other hand, the electronic structure of the oligomers under study has been examined through both the C–C bond-length alternation pattern along the backbone and the distribution of the positive charge among the heterocycles.

All the quantum mechanical calculations were performed with the Gaussian 03 computer program [22].

3. Results and discussion

3.1. Electroactivity of PPy and PNMPy films

PPy and PNMPy films were generated by CA under a constant potential of 1.4 V considering two different polymerization times (θ) for each material: 300 and 60 s. Table 1 lists the thickness (l) of resulting films, the density (ρ) and both n_{ox} and n_{av}. Similar thickness values were obtained from yielded films at each polymerization time, which allows the comparison between the properties of the two conducting polymers.

The number of positive charges per monomer unit, *i.e.* the doping level, determined for electrogenerated PPy and PNMPy by standard ion chromatography on reduced polymer

Table 1
Characteristics of PPy and PNMPy electrogenerated by chronoamperometry: thickness (l; in micrometers) of the films prepared using $\theta = 300$ and 60 s, doping level, n_{ox} and n_{av} (both in electrons), and density (ρ; in grams per centimeter cube)

	l ($\theta = 300$ s)	l ($\theta = 60$ s)	Doping level	n_{ox}	n_{av}	ρ
PPy	2.15	0.38	0.22	1.77	1.55	1.590
PNMPy	3.40	0.79	0.72	2.55	1.83	1.595

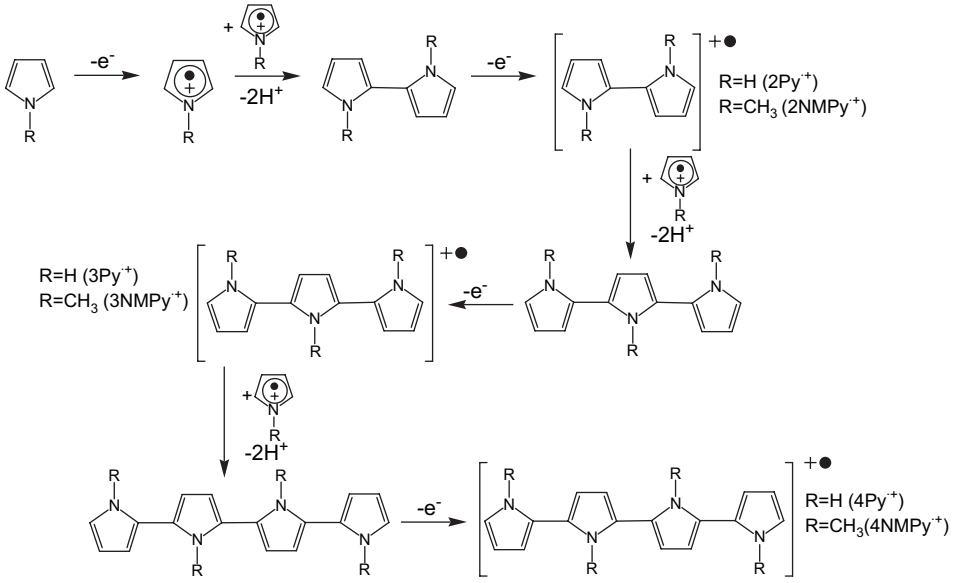

Fig. 1. Mechanism of electropolymerization proposed for Py and NMPy.

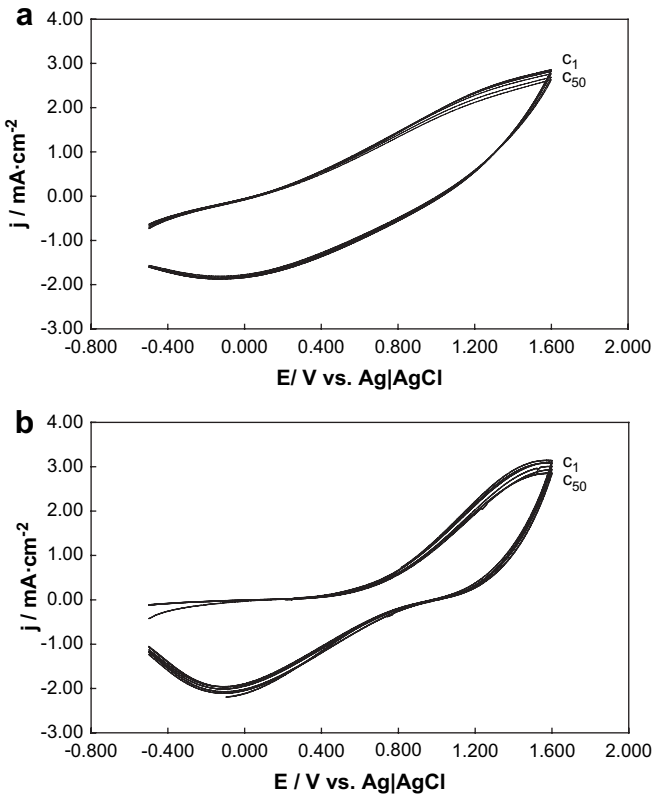

Fig. 2. Control voltammograms for 50 consecutive oxidation–reduction cycles of (a) PPy and (b) PNMPy films on 4 cm^2 steel sheets in acetonitrile with 0.1 M $LiClO_4$, at 100 mV s^{-1} and 25 °C. Initial and final potentials: −0.50 V; reversal potential: 1.60 V. The films were generated for $\theta = 300$ s under the conditions provided in the text. In order to clarify the presentation, only the voltammograms recorded every 10 cycles are displayed. The labels c_1 and c_{50} correspond to the voltammograms recorded in the first and 50th cycles.

samples is 0.72 and 0.22, respectively. The formulas for an oxidized molecule of PPy and PNMPy can be written as

$$\left[\left(PPy^{0.22+}\right)_n\left(ClO_4^-\right)_{0.22n}\right]_{solid}$$

$$\left[\left(NMPy^{0.72+}\right)_n\left(ClO_4^-\right)_{0.72n}\right]_{solid}$$

evidencing that the doping level of the *N*-substituted derivative is considerably higher.

As mentioned in Section 1, the expected value of n_{av} is 2.00 for the formation of an infinite linear molecule from a radical polycondensation mechanism [7,9] (see Fig. 1). However, n_{av} is lower than 2.00 for both PPy and PNMPy. This feature indicates the existence of parallel chemical polymerization reactions based on proton transfer processes during the electrochemical polycondensation. Accordingly, as no electron of the external circuit participates in such chemical processes, which are typically detected in Py and its derivatives [5], the resulting n_{av} values are lower than 2.00. However, the most noticeable result in Table 1 is that both n_{ox} and n_{av} are significantly lower for PPy than for PNMPy. It is usually accepted that the polymer with highest n_{ox} and, especially, n_{av} values also shows the highest degree of ramification and/or cross-linking and, therefore, is least electroactive. Accordingly, the electroactivity of the PNMPy is expected to be significantly lower than that of PPy.

Fig. 2 shows the control voltammograms for 50 consecutive oxidation–reduction cycles of the PPy and PNMPy films prepared using $\theta = 300$ s. As can be seen, no sign of destabilization was detected for PPy, the overlapping between the control voltammograms of first (c_1) and last (c_{50}) oxidation–reduction cycles being almost perfect. Thus, the structure of PPy is suitable to allow the access and escape of dopant ions along the oxidation and reduction processes, respectively. On the other hand, for PNMPy the area of the 50th cycle is about 92% of the area of the first cycle (Fig. 2b). This reduction indicates that the loss of electroactivity is also very small for this polymer, even although the electrostability is slightly lower for PNMPy than for PPy. The overall of these results indicate that PPy and PNMPy films prepared using $\theta = 300$ s involve long and linear polymer chains, and their ability to store charge is not reduced by undesired cross-linking processes. This should be attributed to the lack of short branches in polymer chains able to form cross-links, *i.e.* molecular branches, if exist, are too long.

The control voltammograms for consecutive oxidation–reduction cycles of the PPy and PNMPy films prepared using $\theta = 60$ s are displayed in Fig. 3a and b, respectively. As can be

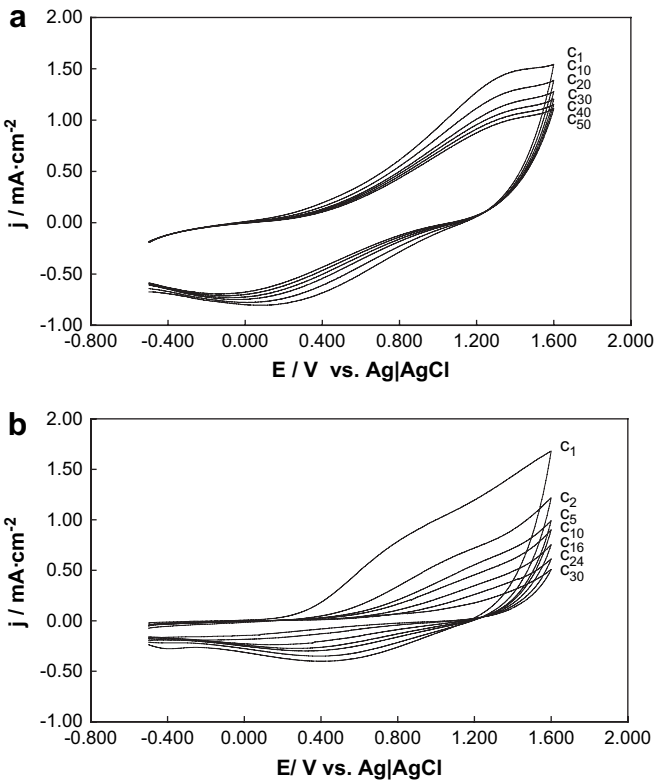

Fig. 3. Control voltammograms for 50 and 30 consecutive oxidation–reduction cycles of (a) PPy and (b) PNMPy films, respectively, on 4 cm^2 steel sheets in acetonitrile with 0.1 M $LiClO_4$, at 100 mV s^{-1} and 25 °C. Initial and final potentials: −0.50 V; reversal potential: 1.60 V. The films were generated for $\theta = 60$ s under the conditions provided in the text. In order to clarify the presentation, only the voltammograms recorded after x oxidation–reduction cycles, which have been labeled as c_x, are displayed.

seen, the electrochemical behavior of these systems is completely different from that recorded for the films generated using $\theta = 300$ s. Specifically, the electrostability of the two materials decreases with θ. Analysis of Fig. 3a shows that the electroactivity of PPy evolves as follows: (a) the area of the first voltammogram decreases ~20% after 20 consecutive oxidation–reduction cycles (c_{20}); and (b) the area of the voltammogram recorded along the 50th oxidation–reduction cycle (c_{50}) is ~30% smaller than that recorded in the first cycle. Accordingly, the ability to store charge showed initially by PPy decreases by only ~10% along the last 30 oxidation–reduction cycles. This feature evidences the formation cross-links in the polymer structure, which occur along the first oxidation–reduction cycles. Presumably, these reactions involve short branches, which are consequence of the small polymerization time. However, after their reaction, long and linear polymer chains dominate the structure of PPy imparting electrostability to the system. Thus, it can be concluded that PPy chains are predominantly linear, even although some degree of branching is evidenced in Fig. 3a.

On the other hand, PNMPy electropolymerized using $\theta = 60$ s shows a significant loss of electroactivity after only two consecutive oxidation–reduction cycles (c_2), *i.e.* the area of the voltammogram decreases by ~35% (Fig. 3b). Moreover, the area of the voltammogram recorded along the 10th (c_{10}) and 30th (c_{30}) cycles is ~60% and ~90% smaller than that recorded in the first cycle, respectively. These results reflect that the PNMPy film prepared using $\theta = 60$ s is predominantly formed by short and branched molecules that easily react forming a significant number of cross-links. Thus, after 30 oxidation–reduction cycles the density of cross-links is so high that the access of the dopant ions into the system is not allowed. Accordingly, the architecture of the molecular chains is different for PNMPy and PPy.

3.2. Theoretical calculations

3.2.1. Dimers

Calculations started considering the reaction of the monomeric unit ($M^{\bullet+}$), which was in the radical cation state, with the monomer (M) to yield the dimer $2M^{\bullet+}$. The reactive site of $M^{\bullet+}$ was the α-position, while M was allowed to react through both the α- and the β-position. Consequently, two dimers, the α,α and α,β, were considered for each system, M = Py or NMPy (Fig. 4). Table 2 lists the relative energies and ε_g values predicted for the α,α and α,β dimers of $2Py^{\bullet+}$ and $2NMPy^{\bullet+}$. As can be seen, the two structures are almost isoenergetic for the former system, while the α,β is clearly favored for the latter one. This is because the steric interactions induced by the *N*-methyl substitution destabilize the growth of the molecular chains through the formation of α,α-linkages. The relative energy calculated for the α,α structure of $2NMPy^{\bullet+}$ (4.6 kcal/mol) was used as the threshold limit to separate low- from high-energy structures in $3M^{\bullet+}$ and $4M^{\bullet+}$ (see below).

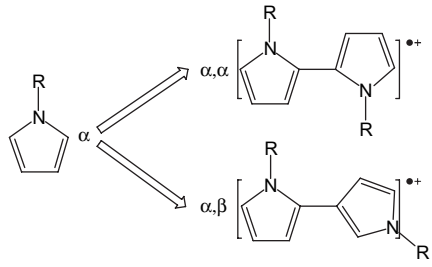

Fig. 4. Structures (α,α and α,β) calculated for $2Py^{\bullet+}$ (R = H) and $2NMPy^{\bullet+}$ ($R = CH_3$).

Table 2
Relative energy (ΔE) and π–π* lowest transition energy (ε_g) of the structures calculated for $2Py^{\bullet+}$ and $2NMPy^{\bullet+}$

System	α,α		α,β	
	ΔE (kcal/mol)	ε_g (eV)	ΔE (kcal/mol)	ε_g (eV)
$2Py^{\bullet+}$	0.2	8.30	0.0	8.51
$2NMPy^{\bullet+}$	4.6	8.25	0.0	8.40

Inspection of the optimized geometries indicated a planar quinoid-like structure with an inter-ring dihedral angle (θ) of 180° in all cases with exception of the α,α dimer of $2NMPy^{\bullet+}$, which is distorted from the planarity ($\theta = -165.0$) to minimize steric repulsions. Thus, the planarity found for $2Py^{\bullet+}$ is fully consistent with previously reported calculations on Py-containing oligomers, which indicated that the *anti-gauche* ($\theta = 152°$) conformation found for the neutral state transforms in *all-anti* ($\theta = 180°$) after oxidation [23–28]. However, although the preferred conformation of neutral NMPy-containing oligomers also corresponds to the *anti-gauche*, the θ value is ~23° smaller than that of Py-containing oligomers [23,28]. Interestingly, $2Py^{\bullet+}$ and $2NMPy^{\bullet+}$ retain such difference due to the repulsive interactions induced by the methyl substituent.

On the other hand, the influence of the reaction positions on ε_g is small but non-negligible. Thus, the largest difference, which corresponds to $2Py^{\bullet+}$, is 0.21 eV. As expected, the lowest ε_g value was obtained for the α,α structure in the two systems under study. However, for each type of inter-ring linkage, the ε_g value calculated for $2Py^{\bullet+}$ is, surprisingly, slightly higher than that obtained for $2NMPy^{\bullet+}$. Thus, as mentioned above, deviations from the planarity are detected in latter compound due to the steric interactions induced by the methyl groups.

3.2.2. Trimers

The two structures calculated for $2M^{\bullet+}$ were used as starting points to generate all the possible structures for the trimer $3M^{\bullet+}$ assuming that the third ring links to the second one, *i.e.* structures derived by linking the third ring to the first one were omitted. The α-, β-, β′- and α′-position of third ring was considered for each of the three reaction sites of the second ring (Fig. 5), the total number of structures calculated for the $3M^{\bullet+}$ with M = Py or NMPy being 2 (structures of dimers) × 3 (reaction sites of the second ring) × 4 (positions of the third ring) = 24.

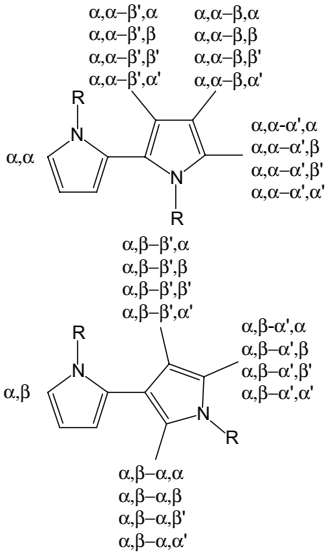

Fig. 5. Structures calculated for $3Py^{\bullet+}$ (R = H) and $3NMPy^{\bullet+}$ ($R = CH_3$). Labels in the reactive positions of the second ring display the linkages considered for the third ring.

The results obtained for $3Py^{\bullet+}$ and $3NMPy^{\bullet+}$ are summarized in Table 3, which lists the structures with relative energies lower than 4.6 kcal/mol. As can be seen, only three and two structures, respectively, are below this threshold limit, while the remaining ones are destabilized by more than 6.1 kcal/mol. In both cases the α,α−α′β structure corresponds to the lowest energy minimum, which indicates that the two systems tend to grow irregularly. However, this tendency is more pronounced for $3NMPy^{\bullet+}$ since in this system the regular structure α,α−α′α is significantly destabilized with respect to the global minimum. Analysis of the optimized inter-ring dihedral angles for the low energy structures listed in Table 3 indicates that $3Py^{\bullet+}$ adopts a perfectly planar *trans* conformation ($\theta = 180.0°$) in all cases, while the structures of $3NMPy^{\bullet+}$ deviate systematically from the planarity, *i.e.* the values of $\Delta\theta = 180.0 - |\theta|$ range from 17° to 19° in all cases.

On the other hand, the influence of the linkage on ε_g is significantly larger in the trimers than in dimers, even though the values listed in Table 3 for the lower energy structures are relatively similar. For $3Py^{\bullet+}$ the largest difference was found between the α,α−β′,α and the α,α−ββ structures (6.97 and 7.93 eV, respectively), while for $3NMPy^{\bullet+}$ the largest difference corresponds to α,α−β′,α and α,α−β,α (7.73 and 7.18 eV, respectively). Thus, the range of variation decreases from 0.94 to 0.55 eV upon the *N*-methylation of the trimers. Furthermore, it is worth noting that the α,α−α′α structure of $3Py^{\bullet+}$, which is unfavored by only 2.0 kcal/mol, shows the lowest ε_g value in Table 3.

Table 3
Relative energy (ΔE) and π−π* lowest transition energy (ε_g) of the structures calculated for $3Py^{\bullet+}$ and $3NMPy^{\bullet+}$ that are below the threshold limit of 4.6 kcal/mol (see text)

$3Py^{\bullet+}$			$3NMPy^{\bullet+}$		
	ΔE (kcal/mol)	ε_g (eV)		ΔE (kcal/mol)	ε_g (eV)
α,α−α′,β	0.0	7.46	α,α−α′β	0.0	7.42
α,α−α′,β′	1.2	7.47	α,α−α′β′	0.6	7.42
α,α−α′,α	2.0	7.34	–	–	–

3.2.3. Linear tetramers

The structures listed in Table 3 for $3Py^{\bullet+}$ and $3NMPy^{\bullet+}$ were used as starting points to generate all the possible structures for the tetramers $4Py^{\bullet+}$ and $4NMPy^{\bullet+}$ assuming that the fourth ring links to the third one, *i.e.* structures derived by linking the fourth ring to the first and second ones were omitted in this stage. The α-, β-, β′- and α′-position of fourth ring was considered for each of the three reaction sites of the third ring (Fig. 6). The total number of structures calculated for the $4Py^{\bullet+}$ was 3 (structures of trimer) × 3 (reaction sites of the third ring) × 4 (positions of the third ring) = 36, while the computed for $4NMPy^{\bullet+}$ was 2 (structures of trimer) × 3 (reaction sites of the third ring) × 4 (positions of the third ring) = 24.

Table 4 shows the structures obtained for $4Py^{\bullet+}$ with relative energies lower than 4.6 kcal/mol. The number of structures below such threshold value is 15 suggesting that the growth mechanism of PPy chains is very complex. However, a detailed inspection of the structures displayed in Table 4 evidences that $4Py^{\bullet+}$ presents an important tendency to form

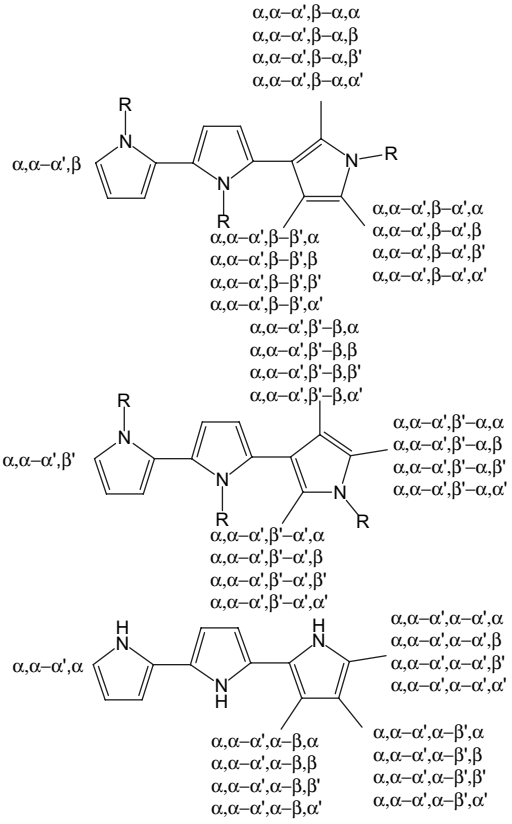

Fig. 6. Linear structures calculated for $4Py^{\bullet+}$ (R = H) and $4NMPy^{\bullet+}$ ($R = CH_3$). Labels in the reactive positions of the third ring display the linkages considered for the fourth ring.

Table 4
Relative energy (ΔE) and $\pi-\pi^*$ lowest transition energy (ε_g) of the structures calculated for $4Py^{\bullet+}$ that are below the threshold limit of 4.6 kcal/mol (see text)

	ΔE (kcal/mol)	ε_g (eV)
α,α–α′,α–α′,β	0.0	6.89
α,α–α′,β′–α′,β	0.3	7.39
α,α–α′,α–α′,β′	0.9	6.93
α,α–α′,α–β,β	1.3	7.43
α,α–α′,β–β′,β	1.9	7.51
α,α–α′,α–α′,α	2.0	6.84
α,α–α′,β–α,β	2.2	7.14
α,α–α′,β–α,β′	2.2	7.34
α,α–α′,β–α,β	2.5	7.34
α,α–α′,α–β,β	2.9	7.33
α,α–α′,β–α′,β	3.0	7.08
α,α–α′,β–β′,α	3.3	7.52
α,α–α′,β′–α′,α	3.4	7.52
α,α–α′,β–α′,β	3.7	7.06
α,α–α′,β′–α,β′	4.2	7.05

irregular linear chains. Thus, although the α,α–α′,α–α′,α is unfavored by 2 kcal/mol only, the lowest energy arrangement displays two α,α-linkages followed by an irregularity that is produced by the last α′β-linkage. Moreover, interestingly the first two linkages are of the α,α type in four of the six structures with lowest relative energies. Examination of the inter-ring dihedral angles indicates that, in some cases, steric clashes between the fourth Py and either the third or the second one induce a *gauche–gauche* conformation in the last dihedral.

On the other hand, analysis of the ε_g values reveals a wide range of variation, *i.e.* 0.68 eV, which can be explained by the electronic structure of the different arrangements. Fig. 7a compares the C–C bond-length pattern along the backbone of the α,α–α′,α–α′,α and α,α–α′,β–β′,α structures, which shows the lowest (6.84 eV) and highest (7.52 eV) ε_g values. Furthermore, the bond-length pattern of the α,α–α′,α–α′,β structure, which is the lowest energy one ($\varepsilon_g = 6.89$ eV), has been also included in such comparison. The regular structure α,α–α′,α–α′,α shows the highest degree of π-conjugation as is reflected by the low variability of the C–C bond lengths. Thus, the length of the inter-ring bonds, which are marked by arrows in Fig. 7a, is relatively similar to that of their neighbor intra-rings bonds. This conjugation is partially reduced in the last ring of the α,α–α′,α–α′,β structure leading to a slight increase of the ε_g value. Finally, it is worth noting that the α,α–α′,β–β′,α structure presents a completely different profile. Thus, the third inter-ring bond length, which connects the third and fourth rings, is 0.051 Å larger than that calculated for the α,α–α′,α–α′,α structure. In opposition, the first inter-ring bond length is 0.022 Å larger for the α,α–α′,α–α′,α structure than for the α,α–α′,β–β′,α one.

The overall of these results explains not only the high ε_g value predicted for the α,α–α′,β–β′,α structure but also the distribution of the positive charge among the four rings of the tetramer. Table 5 provides the charge on each pyrrole ring calculated for selected structures of $4Py^{\bullet+}$. As can be seen, the positive charge is mainly accumulated at the extremes of the oligomer in α,α–α′,α–α′,α, while in α,α–α′,β–β′,α all pyrrole rings are significantly charged.

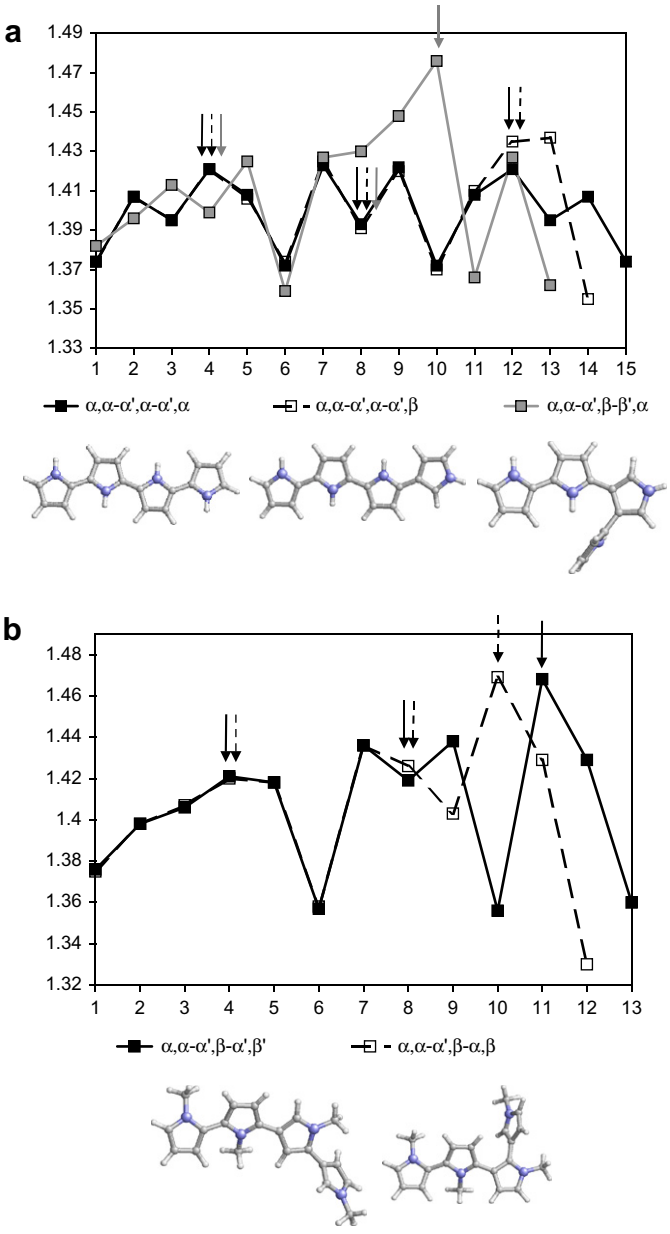

Fig. 7. C–C bond distances (in angstroms) along the backbone of selected structures (see text), which are specifically represented, for (a) $4Py^{\bullet+}$ and (b) $4NMPy^{\bullet+}$. Inter-ring bond lengths are marked with arrows.

Table 6 lists the eight structures obtained for $4NMPy^{\bullet+}$ with relative energies lower than 4.6 kcal/mol. As can be seen, the

Table 5
Charge (in units of electron) on the four pyrrole rings of $4Py^{\bullet+}$ calculated for selected structures

	Py-1	Py-2	Py-3	Py-4
α,α–α′,α–α′,β	0.394	0.084	0.283	0.239
α,α–α′,α–α’,α	0.442	0.058	0.058	0.442
α,α–α′,β–β′,α	0.595	0.354	−0.264	0.315

Table 6
Relative energy (ΔE) and $\pi-\pi^*$ lowest transition energy (ε_g) of the structures calculated for 4NMPy$^{\bullet+}$ that are below the threshold limit of 4.6 kcal/mol (see text)

	ΔE (kcal/mol)	ε_g (eV)
α,α–α′,β–α′,β′	0.0	7.29
α,α–α′,β–α′,β	0.0	7.28
α,α–α′,β–α,β	0.3	7.33
α,α–α′,β–α,β′	0.7	7.33
α,α–α′,β′–α′,β	1.9	7.28
α,α–α′,β′–α′,β′	2.2	7.25
α,α–α′,β′–β,β′	2.8	7.43
α,α–α′,β–α,α′	4.4	7.35

relative energy of four of them is lower than 0.7 kcal/mol. Analysis of such four structures, which are almost isoenergetic, indicates not only a significant tendency to branch but also some important structural similarities. Thus, the linkages that involve the second, third and fourth rings are formed between α (or α′) and β (or β′) positions. As a consequence, the ε_g values of the four structures of lower energy, which are the more accessible ones, are very similar, *i.e.* they differ by less than 0.05 eV. The only structure that forms an α,α′-linkage is the α,α–α′,β–α,α′, whose relative energy (4.4 kcal/mol) is very close to the threshold value.

The C–C bond-length pattern along the backbone of structures α,α–α′,β–α′,β′ and α,α–α′,β–α,β, which are almost identical to those of structures α,α–α′,β–α′,β and α,α–α′,β–α,β′, respectively, is compared in Fig. 7b. As can be seen, the only difference appears in the last fragment of the tetramers, even though the two structures reflect the single bond character of the bond associated to the linkage between the third and fourth rings. Thus, conjugation is restricted to the first two NMPy rings. As a consequence, the positive charge of 4NMPy$^{\bullet+}$ is fundamentally localized in such two rings. This feature is evidenced in Table 7, which displays the charge on the four NMPy rings for the structures of lower energy. The charge of each ring was calculated by summing the Mulliken partial atomic charges associated to all the atoms contained in its ring.

3.2.4. Branched tetramers

The tendency of PPy and PNMPy to form branched structures was investigated by computing new structures for the tetramers 4Py$^{\bullet+}$ and 4NMPy$^{\bullet+}$. As in the previous section, the structures listed in Table 3 for 3Py$^{\bullet+}$ and 3NMPy$^{\bullet+}$ were used as starting points to generate the possible branched structures of the tetramers. However, in this case the fourth ring

Table 7
Charge (in units of electron) on the four *N*-methylpyrrole rings of 4NMPy$^{\bullet+}$ calculated for selected structures

	NMPy-1	NMPy-2	NMPy-3	NMPy-4
α,α–α′,β–α′,β′	0.429	0.338	0.147	0.086
α,α–α′,β–α′,β	0.440	0.332	0.136	0.092
α,α–α′,β–α,β	0.419	0.468	0.019	0.094
α,α–α′,β–α,β′	0.419	0.404	0.055	0.122

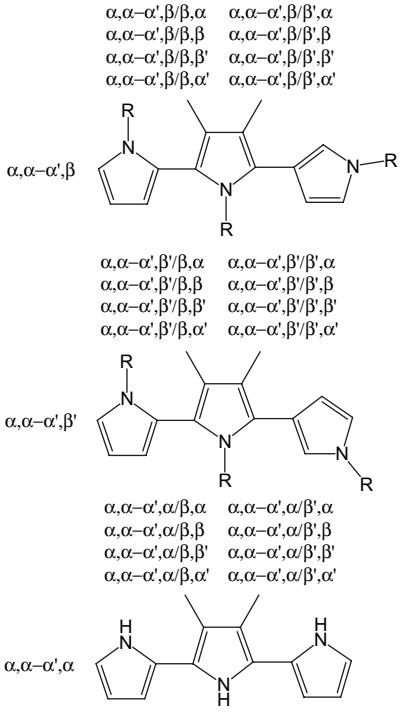

Fig. 8. Branched structures calculated for 4Py$^{\bullet+}$ (R = H) and 4NMPy$^{\bullet+}$ (R = CH_3). Labels in the reactive positions of the second ring display the linkages considered for the fourth ring.

was directly attached to the central one (Fig. 8). The total number of structures calculated for the 4Py$^{\bullet+}$ and 4NMPy$^{\bullet+}$ was 3 (structures of trimer) × 2 (reaction sites of the third ring) × 4 (positions of the third ring) = 24 and 2 (structures of trimer) × 2 (reaction sites of the third ring) × 4 (positions of the third ring) = 16, respectively.

Results indicate that the most stable branched structure of 4Py$^{\bullet+}$, α,α–α′,β/β,β (ε_g = 7.46 eV), is 1.2 kcal/mol less favored than the most stable linear structure (see Table 4). Indeed, the α,α–α′,β/β,β structure, which is displayed in Fig. 9a, is destabilized with respect to three linear structures. The rest of the optimized branched structures are unfavored by more than 3 kcal/mol with respect to the α,α–α′,α–α′,β linear structure. The overall of the theoretical results obtained for *n*Py$^{\bullet+}$ is fully consistent with the experimental results reported above for PPy. Thus, this polymer exhibits a very low tendency to form branched molecular chains and, therefore, to cross-link.

On the other hand, the α,α–α′,β′–β′,β′ branched structure of 4NMPy$^{\bullet+}$ (ε_g = 7.38 eV) is 0.9 kcal/mol more stable than the α,α–α′,β–α′,β′, which is the lowest energy linear structure (see Table 6). In this branched structure, the steric repulsions induced by the methyl side groups are clearly minimized since the four *N*-methylpyrrole rings are located at different plains (Fig. 9b). On the other hand, the α,α–α′,β/β′,β′ (ε_g = 7.36 eV) is less stable than the lowest energy linear structure by only 0.4 kcal/mol. This structure is destabilized with respect to the α,α–α′,β′–β′,β′ one by the unfavorable interactions between the third and fourth NMPy rings (Fig. 9c). The low tendency of *n*NMPy$^{\bullet+}$ to grow forming

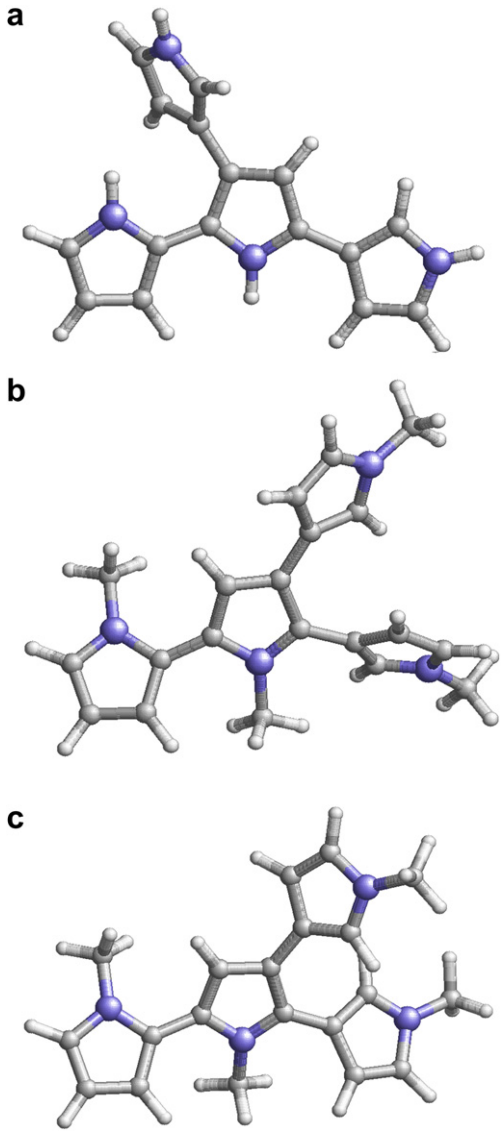

Fig. 9. Molecular structures of selected branched oligomers: (a) α,α–α′,β/β,β for $4Py^{\bullet+}$; (b) α,α–α′,β–α′,β′ for $4NMPy^{\bullet+}$; and (c) α,α–α′,β′–β′,β′ for $4NMPy^{\bullet+}$.

linear chains as well as the remarkable stability of the branched structures is fully consistent with the low electrostability detected for PNMPy.

4. Conclusions

In this work we compare the formation of cross-links in PPy and PNMPy performing both experimental and theoretical studies. PPy and PNMPy were generated electrochemically under a constant potential of 1.4 V. Cyclic voltammograms recorded along consecutive oxidation–reduction cycles indicated that PNMPy is much less electrostable than PPy since the formation of cross-links in the former material makes difficult the access of the dopant anions during of the oxidation processes. This was especially evident for the PNMPy films electrogenerated using $\theta = 60$ s. This material was predominantly formed by short and branched polymer chains, which easily give place to cross-linking.

On the other hand, quantum mechanical calculations on $n\text{Py}^{\bullet+}$ and $n\text{NMPy}^{\bullet+}$ oligomers with $n = 2–4$ allowed to extract two important conclusions. First, the tendency of polymer chains to grow regularly during the electropolymerization process is significantly higher for PPy than for PNMPy. Thus, although calculations on $n\text{Py}^{\bullet+}$ show that chains grow with some defects, α,α-linkages are rarely found in short NMPy-containing chains. Probably, this conclusion is only valid for short polymer chains since the influence of environmental effects, *e.g.* neighboring chains, previous formation of branches, etc, will increase with the number of electropolymerization stages. The second conclusion involves the branching of the chains: for $4NMPy^{\bullet+}$ the branched architecture is more stable than linear one, while the stability order is exchanged for $4Py^{\bullet+}$. This is fully consistent with the experimental results presented in this work.

After a careful examination of the results presented in this work, we conclude that the differences found between PPy and PNMPy are not due to electronic effects induced by the *N*-methylation. The high tendency of NMPy-containing chains both to form branches and to grow irregularly is fundamentally due to the steric effects produced by the methyl group. Thus, PNMPy molecular chains minimize such steric repulsions by forming branches, reducing the formation of α,α-linkages and distorting the inter-ring dihedral angles from planarity.

Acknowledgements

This work has been supported by MCYT and FEDER with Grant MAT2006-04029. Authors are indebted to the Centre de Supercomputació de Catalunya (CESCA) for computational facilities.

References

[1] Lukkari J, Tuomala R, Ristimaki S, Kankare J. Synth Met 1992;47:217.
[2] Lukkari J, Kankare J, Visy C. Synth Met 1992;48:181.
[3] Lukkari J, Alanko M, Pitkänen V, Kleemola K, Kankare J. J Phys Chem 1994;98:8525.
[4] Visy C, Lukkari J, Kankare J. Synth Met 1997;87:81.
[5] Sadki S, Schottland P, Brodie N, Sabouraud G. Chem Soc Rev 2000;29:283.
[6] Funt BL, Diaz AF. Organic electrochemistry: an introduction and a guide. New York: Marcel Dekker; 1991. p. 1337.
[7] Geneis EM, Bidan G, Diaz AF. J Electroanal Chem 1983;149:101.
[8] Ocampo C, Oliver R, Armelin E, Alemán C, Estrany F. J Polym Res 2006;13:193.
[9] Vashanta VS, Phani KLN. J Electroanal Chem 2002;520:79.
[10] Estrany F, Oliver R, Cabot P, Brillas E. Eur Polym J 2006;42:563.
[11] Oliver R, Muñoz A, Ocampo C, Alemán C, Armelin E, Estrany F. Chem Phys 2006;328:299.
[12] Lee H, Yang H, Kwak J. J Electroanal Chem 1999;468:104.
[13] Redondo MI, Sánchez de la Blanca E, García MV, Raso MA, Tortajada J, González-Tejera MJ. Synth Met 2001;122:431.
[14] Brillas E, Oliver R, Estrany F, Rodríguez E, Tejero S. Electrochim Acta 2002;47:1623.
[15] Waltman RJ, Bargon J. Can J Chem 1985;64:76.
[16] Waltman RJ, Bargon J. Tetrahedron 1984;40:3963.

[17] Hariharan PC, Pople JA. Theor Chim Acta 1973;28:213.
[18] Alemán C, Domingo V, Fajarí Ll, Julià L, Karpfen A. J Org Chem 1998;63:1041.
[19] Alemán C, Casanovas J. J Phys Chem A 2004;108:1440.
[20] Bertrán O, Pfeiffer P, Torras J, Armelin E, Estrany F, Alemán C. Polymer 2007;48:6955.
[21] Alemán C, Armelin E, Iribarren JI, Liesa F, Laso M, Casanovas J. Synth Met 2005;149:151.
[22] Frisch MJ, Trucks GW, Schlegel HB, Scusseria GE, Robb MA, Cheeseman JR, et al. Gaussian 03, revision B.02. Pittsburgh, PA: Gaussian, Inc.; 2003.
[23] Gatti C, Frigerio G, Benincori T, Brenna E, Sannicolò F, Zotti G, et al. Chem Mater 2000;12:1490.
[24] Duarte HA, Duani H, De Almeida WB. Chem Phys Lett 2003; 369:114.
[25] Kofranek M, Kovar T, Kaprfen A, Lischka H. J Chem Phys 1992; 96:4464.
[26] Aleman C. Macromol Theory Simul 1997;8:39.
[27] Hutchison GR, Ratner MA, Marks TJ. J Phys Chem A 2002;16: 10596.
[28] Casanovas J, Cho LY, Ocampo C, Alemán C. Synth Met 2005; 151:239.